Journal of Applied Polymer Science

Effect of the compatibility on dielectric performance and breakdown strength of poly(vinylidene fluoride)/low-density polyethylene blends

Xiang Lin,[1] Li-Li Fan,[1] Jun Zhao,[1] Zhi-Min Dang,[1] Dong-Yun Ren[2]

[1]Department of Polymer Science and Engineering, School of Chemistry and Biological Engineering, University of Science and Technology Beijing, Beijing 100083, China

[2]College of Mechanical and Electrical Engineering, Beijing University of Chemical Technology, Beijing 100029, China

Correspondence to: Z. M. Dang (E-mail: dangzm@ustb.edu.cn) and D. Y. Ren (E-mail: dongyunr@163.com)

ABSTRACT: Immiscible polymer blends with high dielectric constant (ε) and improved breakdown strength (E_b) performance were obtained by composing poly(vinylidene fluoride) (PVDF) with low-density polyethylene (LDPE) or the LDPE grafted with maleic anhydride (LDPE-*g*-MAH) through melt-blending way. The dielectric properties of these blends were emphasized for considering the compatibility effect on the energy storage application. Interface morphology, co-continuity behavior, and grafted ratio were simultaneously investigated to detect the compatibility enhancement after introducing MAH. Results showed that the MAH positively improved the dielectric properties. Both the measured E_b of PVDF/LDPE and PVDF/LDPE-*g*-MAH blends showed a minimum value at $v^{PVDF} = 50$ vol % because of the worst compatibility; meanwhile, higher E_b of PVDF/LDPE-*g*-MAH than that of PVDF/LDPE blend was observed owing to the better compatibility. For considering the effect interface morphology on the dielectric performance, layer-structure films composing with pure PVDF and LDPE layers were further constructed and studied. It was revealed that the layered structure could be treated as a helpful way to improve ε and E_b for immiscible polymer blends. © 2015 Wiley Periodicals, Inc. J. Appl. Polym. Sci. **2015**, *132*, 42507.

KEYWORDS: blends; compatibilization; dielectric properties

Received 21 March 2015; accepted 16 May 2015

DOI: 10.1002/app.42507

INTRODUCTION

Dielectric polymeric materials used for energy storage have attracted increasing interests owing to their unique properties,[1,2] such as high insulating resistance, high breakdown strength (E_b), low dielectric loss tangent (tanδ), high flexibility and perfect processability, and effective cost.[3,4] For instance, polypropylene (PP),[5–7] polyethylene (PE),[8,9] polystyrene (PS),[10] poly(ethylene terephthalate) (PET),[11] poly(methyl methacrylate) (PMMA),[12] poly(vinylidene fluoride) (PVDF),[13,14] and polyimide (PI)[15–17] are among the most widely used polymer dielectric materials at present. Especially, PVDF presents relatively high dielectric constant (ε) of *ca.* 8–10 at room temperature.[18] Disadvantages, however, are also revealed from these dielectric polymers, of which the low ε or the high tanδ is the most significant. Introducing additive nanofillers to these dielectric polymers is a widely used strategy to conquer this problem, in which the high-ε ceramics[19–22] or high-conductivity (σ) metal particles[23,24] or carbon materials[25–28] are usually adopted as the ideal candidates. It should be noted that the intrinsic properties of each component and the processing conditions could strongly determine the internal microstructure and the final properties of the composites. However, the polymeric materials described above also present some uncompromised predicaments. Highly immiscible filler, needed for enhancing ε, seriously deteriorate the processability, the mechanical properties and the surface quality. Therefore, it is of great importance to develop polymer blends with high dielectric performance.

As a new strategy, PVDF or its copolymers are becoming the ideal fillers instead of traditional inorganic additives for the dielectric applications. The PVDF and its copolymers are usually blended with polyamide 11,[29] PI,[30] PP,[31,32] and PS[33] for achieving all-organic composites with both high ε and low tanδ. Dang *et al.*[31] successfully improved the dielectric performance of PP only by using PVDF. Apart from the effective enhancement of ε, the tanδ of the blends was still at a low level (<0.05), which satisfied a series of requirements in practical applications. Dang *et al.* further suggested that the additive compatibilizer was mainly found around the interfaces between PP and PVDF and perhaps some was dispersed within the PP phase. The existence of PP-g-MAH could effectively improve the interface interaction and compatibility between PVDF and PP, subsequently resulting in an increase of ε. Effect of mixing process on ε of the typical

© 2015 Wiley Periodicals, Inc.

immiscible blend PVDF/PP was investigated previously.[32] Lower E_b of the blends than the pure components was attributed to the voids produced in the system because of the poor compatibility between components was proposed. For the PVDF/PP blends with 39.7 vol % PP, the E_b monotonically increased with increasing mixing time. After introducing the compatibilizer iPP-g-MAH, a low content of 9.6 vol % caused a slight increase of the E_b, but a higher content of *ca.* 18.3 vol % decreased the E_b.

In this work, PVDF/LDPE blends were systemically studied for finding the potentials of improved dielectric performance and effective cost. The ε and E_b are two important indexes considering for enhancing the maximum energy storage density (U_m); otherwise, the ε is correlated reciprocally with the E_b. The compatibility effect and interface morphology and the effect of both concentrations of PVDF and MAH on the dielectric properties were emphasized. Modified LDPE with MAH was adopted aiming to enhance interface interaction between PVDF and LDPE phases. Lower E_b of the blends than that of the pure components could be attributed to the defect voids because of the poor compatibility between the two components. Therefore, the measured E_b of PVDF/LDPE and PVDF/LDPE-*g*-MAH blends both reach a minimum for the $v^{PVDF} = 50$ vol % because of worse compatibility with internal defects. Higher E_b of PVDF/LDPE-g-MAH than that of PVDF/LDPE were clearly observed due to the better compatibility. This was also identified in the layered structure films, which was found to be helpful to increase ε and E_b due to the decrease of internal defects.

EXPERIMENTAL

Materials

A commercial PVDF (FR901, Shanghai 3F New Materials Company) with a density of 1.78 g/cm^3 and a melt flow index of 26 g (10 min)$^{-1}$ was used in this work. The LDPE (LD100BW, Sinopec) pellets with a density of 0.923 g/cm^3 and a melt flow index of 2.0 g (10 min)$^{-1}$ was selected for the composite cooperation. MAH was purchased from Xilong (China) Chemical Ind., Co., and dicumyl peroxide (DCP) was supplied by Shanghai Crystal Pure Reagent Co. Styrene, used as the dispersant, with a relative density of 0.906–0.909 g/cm^3 was supplied by Tianjin Jinke Chemical Research Institute, and the solvents, including dimethylformamide (DMF, AR) and xylene (AR), were purchased from Beijing Chemical Company (China).

Sample Preparation

A weight proportion of dried LDPE, MAH, DCP, and styrene as 91.7 : 4 : 0.3 : 4 (wt %) was applied and compounded by using a batch mixer (Thermal Scientific Haake Lab, Germany) at 160°C and 100 rpm for 15 min for getting LDPE grafted with MAH.[34] Dried PVDF and LDPE pellets were melt blended through the Haake mixer at 180°C for 15 min. For investigating the compatibilization effect, LDPE-*g*-MAH was used as compatibilizer to replace the same amount of LDPE. Films of PVDF/LDPE-*g*-MAH and PVDF/LDPE blends were molded by hot-compressing at 180°C and 20 MPa for subsequent measurements.

Characterizations

Films from grafted LDPE-*g*-MAH and pure LDPE were hot compressed with thickness of *ca.* 30–60 μm. The grafting effect was detected by using the Fourier Transform Infrared Spectroscopy (Nicolet 6700 FT-IR, Thermo Scientific). Samples of PVDF/LDPE and PVDF/LDPE-*g*-MAH for scanning electron microscope (SEM) detection should be fractured in liquid nitrogen in advance for getting undamaged fractured surface. Then LDPE or LDPE-*g*-MAH was extracted by xylene to observe the dispersion of two components clearly. All the extracted samples were dried completely in vacuum oven at 80°C. Sputter-coating with Pt was conducted before morphology observations on the S4700 SEM (Hitachi, Japan) running at an accelerating voltage of 20 kV.

PVDF/LDPE (PVDF/LDPE-*g*-MAH) and monolayer (tri-layer) PVDF/LDPE blends thin films prepared by hot pressing should be coated with copper by using high-vacuum resistance evaporation coating device ZHD-300 (China). All the dielectric measurements were performed on the Agilent 4294A impedance analyzer (USA) at room temperature over the frequency range of 10^2-10^6 Hz.

Differential scanning calorimeter (DSC) measurements were performed by using a DSC-60 (Shimadzu, Japan) within nitrogen atmosphere. Samples were dried in a vacuum oven at 80°C before they were sealed in aluminum crucibles and were heated from 50 to 220°C at 10.0°C/min.

Compressed films of PVDF/LDPE(PVDF/LDPE-*g*-MAH) and PVDF/LDPE blends with monolayer or trilayer structure, coated by copper with 30–50 μm thickness, were prepared for the electrical breakdown strength measurements by using a high-voltage instrument (J-Trek, America) in AC style. The electrodes were dipped in the silicone oil to prevent flashover and discharge. Each sample was measured for 10 times at different locations.

RESULTS AND DISCUSSION

Grafting and Co-Continuity Analysis

Predetermined amount of solid potassium hydroxide (KOH) and hydrochloric acid (HCl) solution were used as standard solutions with $C_{KOH} = 0.0162$ mol/L ($PH_{KOH} = 12.21$) and $C_{HCl} = 0.0128$ mol/L ($PH_{HCl} = 1.89$). For ensuring KOH reacting with MAH completely, grafted LDPE sample was dissolved in xylene at 95°C and refluxed for 120 min and then excessive KOH-ethanol solution was used, which was finally consumed by the HCl solution through titrating method. Here, the grafting ratio (G) can be calculated as:

$$G = \frac{C1V1\text{-}C2V2}{W} \times 98 \times 100\% = 5.75\%, \quad (1)$$

where C_1, V_1, and C_2, V_2 are the concentrations and volumes of standard solutions of KOH and HCl, respectively. W is the weight amount of MAH. The obtained graft ratio is in the middle level, compared with *ca.* 1.0% (the lowest) and *ca.* 8.5% (the highest).

After excluding the unreacted MAH with KOH solution and further purification, the grafting effect was detected by FTIR, as shown in Figure 1. The peaks at *ca.* 1440 and 2870 cm^{-1} reflect the structure of –CH_2–CH_2– and the peak at *ca.*1780 cm^{-1} can be assigned to the stretching of C═O, which can only be found with a effective reaction after MAH grafting to LDPE. The

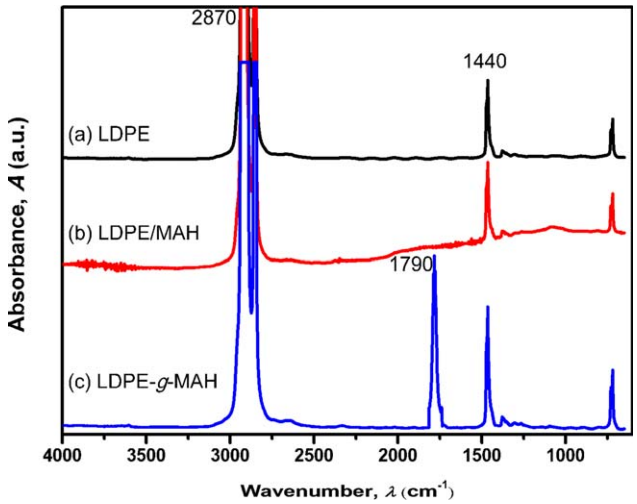

Figure 1. FTIR characterizations of grafting effect. [Color figure can be viewed in the online issue, which is available at wileyonlinelibrary.com.]

unique peak at *ca.*1780 cm^{-1} [Figure 1(c)], indicating the successful carbonylation of LDPE, which can neither be found in the pure LDPE nor in the mixture of LDPE/MAH without the initiator DCP [Figure 1(b)].

For further considering the effect of MAH and the immiscibility between PVDF and LDPE, thermal measurements were further performed by using DSC for the two blend systems: PVDF/LDPE and PVDF/LDPE-g-MAH, as shown in Figure 2. The two unique endothermic [Figure 2(a)]/exothermic [Figure 2(b)] peaks shown in each melting process indicate no chemical reaction between PVDF and LDPE during the blends preparation. Although the melting temperature (T_m) and crystallization temperature (T_c) of LDPE or PVDF seem to be the same, hardly changing with v^{PVDF}, the crystallinity of PVDF/LDPE-*g*-MAH systems presents an reduction in contrast with PVDF/LDPE, which implies a breakage of the crystalline perfection owing to the introduction of MAH [Figure 2(b)]. After the v^{PVDF} reaching to 70%, the melting peak of the LDPE becomes weak and crystallinity of PVDF increases significantly with the help of MAH [Figure 2(a)]. However, for the system of 50/50, both the crystallinity of PVDF and LDPE decrease simultaneously as the effect of MAH. This is because the successful introduction of the MAH enhances the molecular polarity of LDPE, leading to a compatibility improvement between PVDF and LDPE-*g*-MAH according to the principle of "like dissolves like".

Furthermore, interface morphologies of PVDF/LDPE and PVDF/LDPE-*g*-MAH are given through the SEM observation, as shown in Figure 3. For an immiscible blend, it can be sure that the compatibility within co-continuity window is worse than that with the other contents in which typical insular structures are presented. In Figure 3, the clear and smooth interface between PVDF and LDPE without MAH [Figure 3(a)] and confusing interface with MAH [Figure 3(b)] are obviously observed. This indicates that the MAH modification actually improves the compatibility between PVDF and LDPE owing to the increases of polar interaction and binding force around interface. This enhancement of the bonding interaction also plays a positive effect on the mechanical properties, which also represents the compatibility increase, as shown in Figure 4. Higher maximum tensile forces of the modified samples than those of the unmodified samples are revealed. The tensile samples were hot compressed with a dumb-bell shape and a geometrical dimension of 17.5 (length) × 4 (width) × 2 (thickness) mm.

As to the effect of v^{PVDF}, however, it is difficult to judge which systems are more compatibilized only by SEM observation. As documented in literature,[32] selective solvent extraction was further used to measure the co-continuity window of the blends. A piece of PVDF/LDPE blend with a mass of *ca.* 0.10–0.15 g was put into a flask and immersed in comparatively large volume of the selective solvent for fully dissolving the selected phase. Quantitative data on the extent of continuity (x_c) of the phase could be given as:

$$x_c = \frac{w_i - w_f}{w_i} \times 100\%, \quad (2)$$

where w_i and w_f are the weight of one component presented in the sample before and after extraction, respectively. The x_c represents the fraction of a phase, which is continuous in the

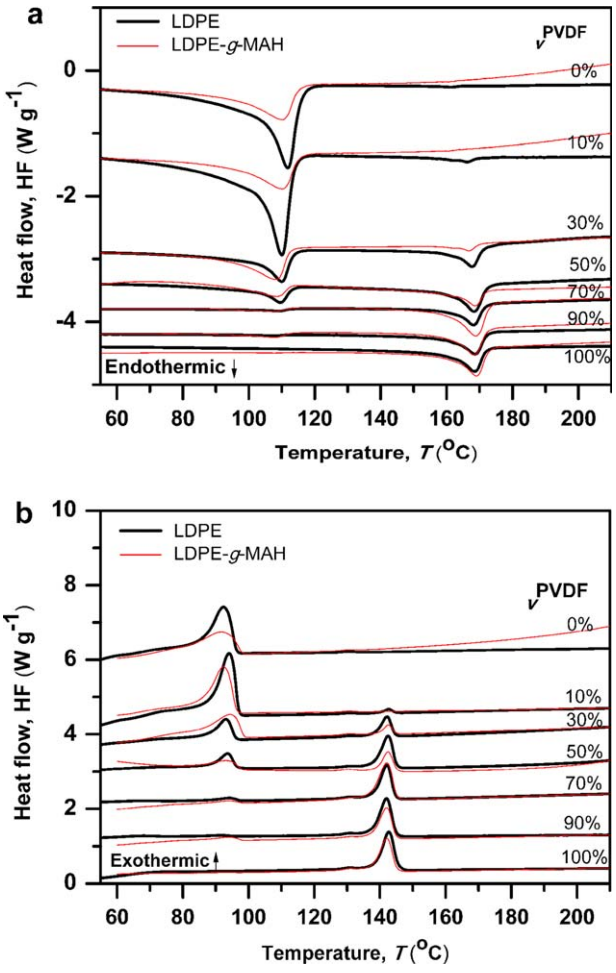

Figure 2. Heat flow traces of PVDF/LDPE and PVDF/LDPE-*g*-MAH blends with varied v^{PVDF}. [Color figure can be viewed in the online issue, which is available at wileyonlinelibrary.com.]

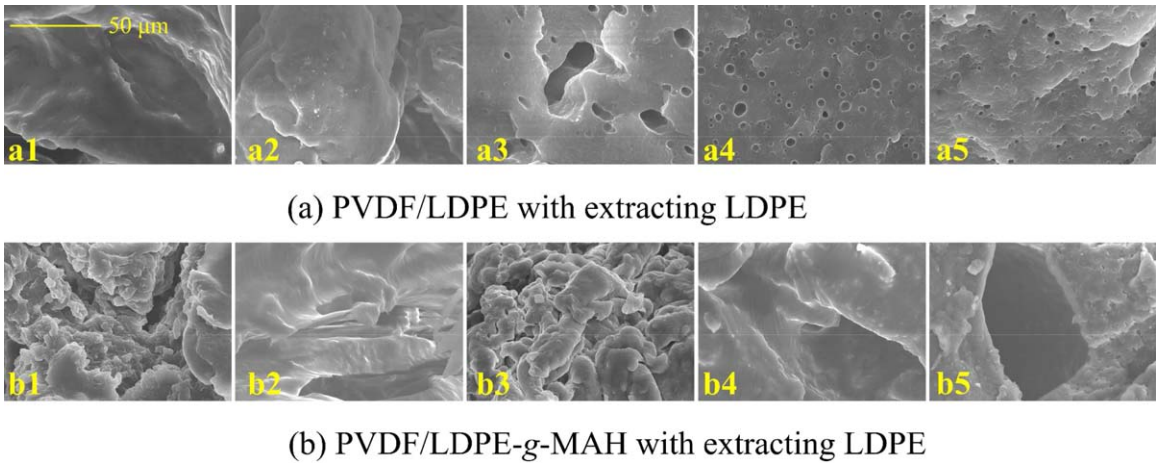

Figure 3. SEM micrographs: PVDF/LDPE (a) and PVDF/LDPE-*g*-MAH (b). PVDF volume fractions from a1 (b1) to a5 (b5) are 10, 30, 50, 70, and 90%, respectively. [Color figure can be viewed in the online issue, which is available at wileyonlinelibrary.com.]

sample. The reported value was calculated from the average of four samples with the same compositions, as shown in Figure 5. The continuity of PVDF increases significantly with the increase of v^{PVDF} up to 50 vol % after which a plateau is obtained, whereas it is vice versa for the LPDE. The v^{PVDF} region between the two vertical dashed lines indicates the range of co-continuity window, which is shown with the PVDF content of 30–50 vol % (Figure 3. (a2, a3, and b2, b3)]. Within the co-continuity window, one of the two phases of PVDF or LDPE is permeated reciprocally into the other. For example, the PVDF, acted as the insular role, is well dispersed in the LDPE phase when the v^{PVDF} is below 30 vol %. The dispersed PVDF can be treated as an additive with high dielectric constant. But when the v^{PVDF} is up to 50%, this situation is totally reversed. Although this is not useful to enhance the compatibility within the co-continuity window, it will effectively change the interfacial surface and affect the dielectric performance significantly. In addition, it should be noted that the x_c ranging from *ca.* 30–50 vol % is narrower than that of the previously reported PVDF/PP blend[32] in which the window of it is *ca.* 20–50 vol % of PVDF. This suggests that there is a better compatibility between PVDF and LDPE than that of PVDF/PP.

Dielectric Measurements

Frequency dependences of ε and tanδ of PVDF/LDPE and PVDF/LDPE-*g*-MAH blends were presented in Figure 6. It can be seen that for pure LDPE, both ε and tanδ are independent of frequency over the frequency range of 10^2-10^6 Hz. With increasing v^{PVDF}, the ε of PVDF/LDPE and PVDF/LDPE-*g*-MAH blends increase differently. Despite a variety of models based on different assumptions were proposed to elaborate the ε of mixtures or blends, the typical equation based on parallel and series alignments was widely used. The ε of two models can be calculated as:

$$\varepsilon=(\varepsilon_a^n v_a+\varepsilon_b^n v_b)^{1/n}, \quad (3)$$

where ε_a, v_a, and ε_b, v_b are the dielectric constant and the volume fractions of components A and B, respectively. Index n is a fitting factor and varies from 1 (for parallel alignment) to −1 (for series alignment). Generally, the ε of real mixtures should

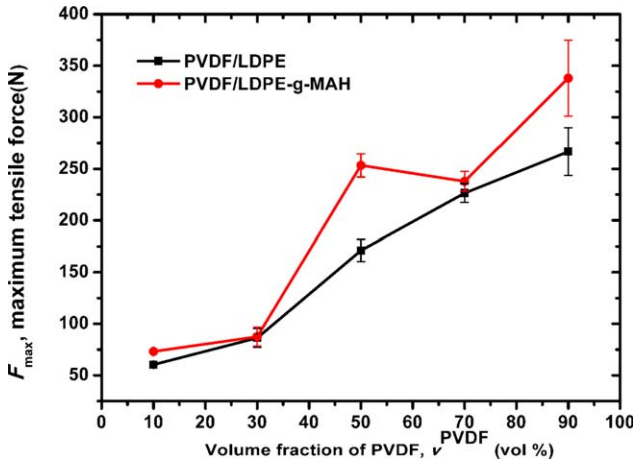

Figure 4. Comparison of the maximum tensile force between the modified and unmodified samples. [Color figure can be viewed in the online issue, which is available at wileyonlinelibrary.com.]

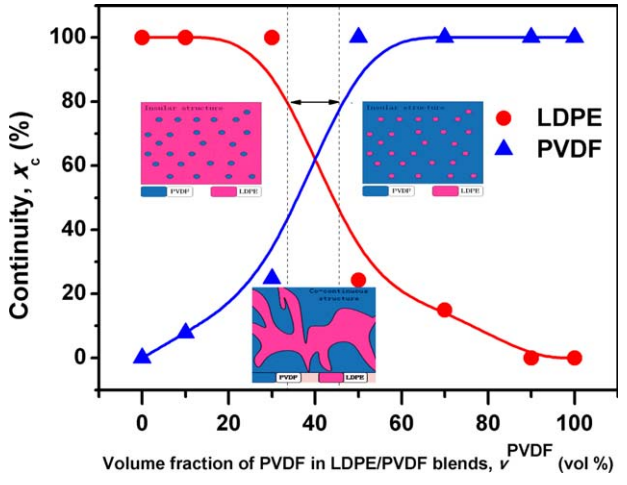

Figure 5. The phase-continuity of both PVDF and LDPE as a function of v^{PVDF}. [Color figure can be viewed in the online issue, which is available at wileyonlinelibrary.com.]

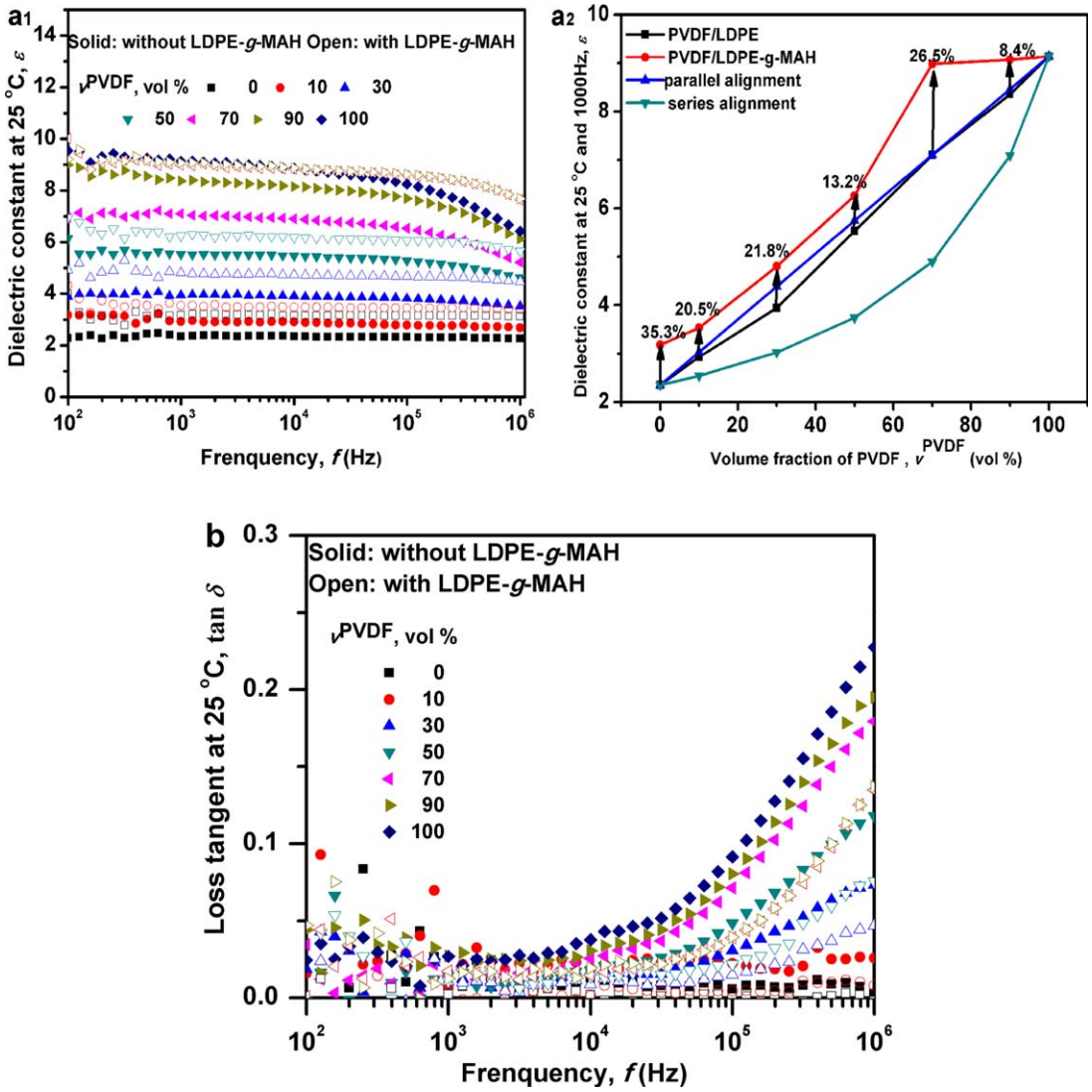

Figure 6. Frequency dependence of ε and tanδ of PVDF/LDPE and PVDF/LDPE-*g*-MAH blends. [Color figure can be viewed in the online issue, which is available at wileyonlinelibrary.com.]

fall in between two models. In Figure 6(a_2), the measured ε of the PVDF/LDPE blends with/without MAH modification are respectively compared with the parallel and series alignment models at room temperature and 1 kHz [Figure 6(a_1)]. The frequency dependence of ε and tanδ of PVDF/LDPE and PVDF/LDPE-*g*-MAH blends is compared, mainly focusing on the effect of MAH modification. For the PVDF/LDPE blends, linear distribution of the ε is observed, which is rather closing to the parallel alignment line [Figure 6(a_2)]. That means the dielectric performance of PVDF/LDPE blends can be modeled by the parallel alignment. Benefited from the introduction of MAH, the ε of LDPE-g-MAH (i.e., $\nu^{PVDF} = 0\%$) increases by *ca.* 35% because the orientated polarization of LDPE molecules under external electric field is significantly strengthened after grafting the polar molecule (MAH). The existence of MAH effectively improves the interface interaction, subsequently resulting in a higher increase of ε on different levels. Meanwhile, all the tanδ decreases obviously with the decrease of PVDF volume owing to the higher tanδ of the PVDF itself. Lower tanδ is found for those samples modified with MAH because of the decrease of interfacial defects and the increase of compatibility. In addition, the tanδ increases with the frequency is due to the dielectric relaxation of the polar PVDF chains, especially at high frequency. Movements of these polar molecular groups present hysteretic behavior at high frequency, which can be largely covered under low frequency.

To further identify the compatibility effect affecting dielectric performance, a simple and effective way to moderate the interface effect was developed with trilayered structure films, which were constructed by blend layers or pure layers, respectively, as shown in Figure 7. Tri-layered film composed by pure PVDF or LDPE is the same to the single layer, treated as a 0% increase in ε. To better control the content of each composition, weight fraction (wt %) was adopted in calculating concentrations. It should be noted that the interface effect between PVDF and LDPE can only be found around overlying surface for the films

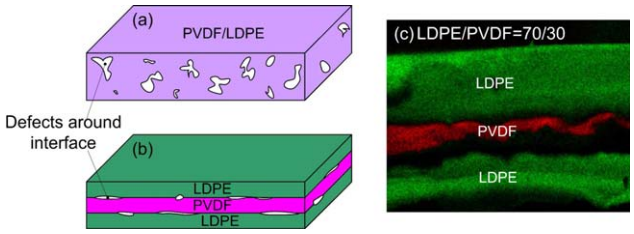

Figure 7. Schematics of the interface defect distribution in mono-layered (a) and tri-layer film (b) and an example of SEM-EDS graphics of the tri-layer structure (c) of LDPE (70)/PVDF (30) blend. [Color figure can be viewed in the online issue, which is available at wileyonlinelibrary.com.]

constituting single pure layers, but for the layered films constructed by single blend layers the interface effect could be full of the whole film. Thus, the layered structure with single pure layer is helpful for decreasing defects and increasing dielectric property, as shown in Figure 8.

An example of the frequency dependence of ε and tanδ of monolayer and trilayer PVDF/LDPE films is given in Figure 8. Compared with the monolayered films of PVDF/LDPE blends, a positive enhancement of the ε and a slight reduction of the tanδ are observed for the trilayer PVDF/LDPE films. Owing to their poor compatibility, the binding force around boundary surface is weak, which induce to weak interface interaction and limited enhancement for the dielectric properties.

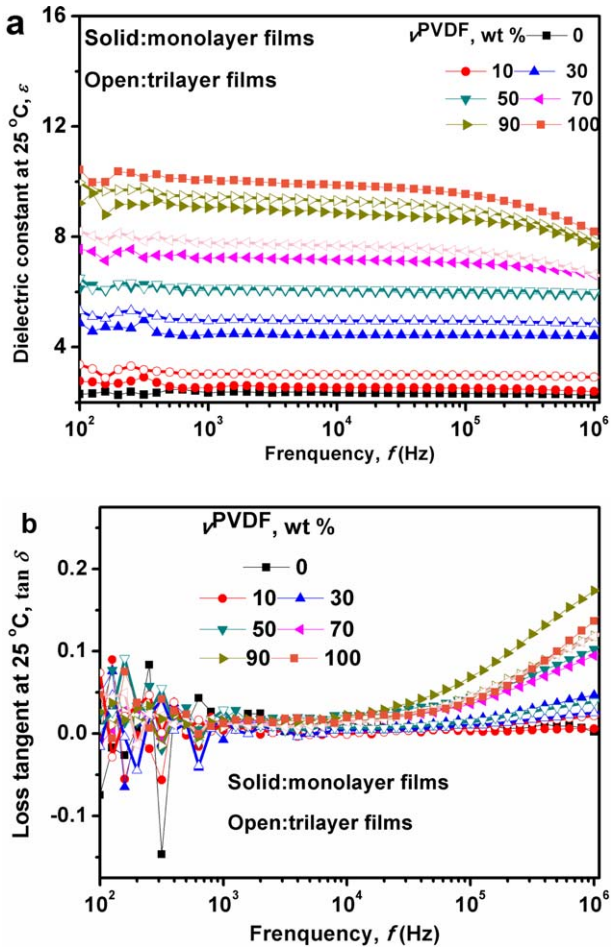

Figure 8. Frequency dependence of ε and tanδ of mono-layer and tri-layer films of PVDF/LDPE. [Color figure can be viewed in the online issue, which is available at wileyonlinelibrary.com.]

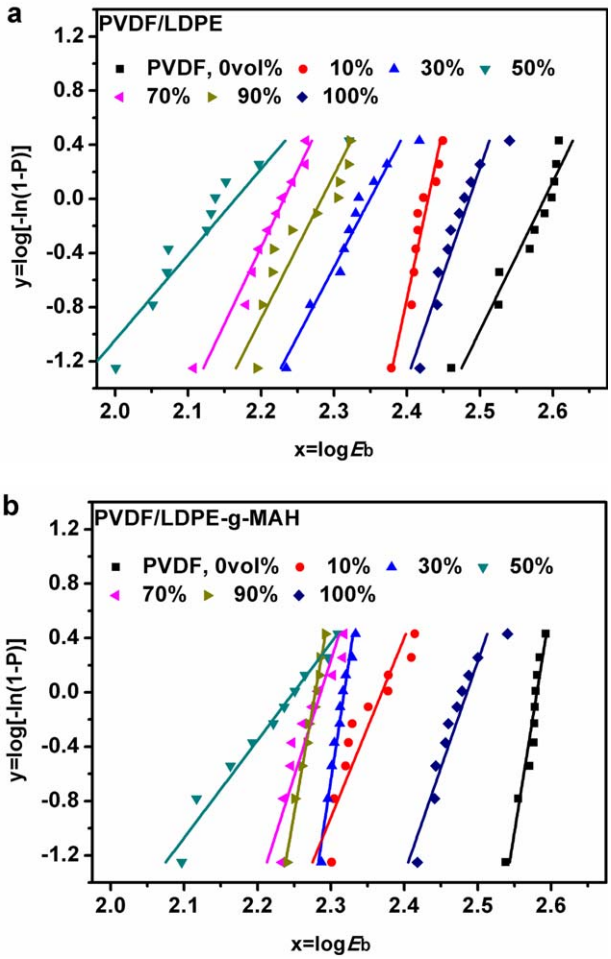

Figure 9. Weibull distribution for E_b of PVDF/LDPE and PVDF/LDPE-*g*-MAH blends. [Color figure can be viewed in the online issue, which is available at wileyonlinelibrary.com.]

Electrical Breakdown Strength Measurements

Figure 9 presents the Weibull distribution of E_b of PVDF/LDPE and PVDF/LDPE-*g*-MAH blends on the ν^{PVDF}. Weibull distribution principle, proposed by the Waloddi Weibull in 1939, is a reliable analysis method for estimating the average data. In this work, it was used to evaluate the breakdown probability of sample within electric field. About 10 samples for each average data were especially adopted. The E_b of measured samples is relative to the Weibull distribution regularity by means of the formula as:

$$P=1-\exp\left[-\left(\frac{E_b}{E_0}\right)^{\beta}\right] \Rightarrow \log\left[-\ln\left(1-P\right)\right]=\beta\log\left(E_b\right)-\beta\log\left(E_0\right), \quad (4)$$

where P is breakdown probability, β is shape parameter, and E_b, E_0 are measured and calculated breakdown strength, respectively, as shown in Table I. The narrower data dispersion of E_b

Table I. The ε, E_0, and U_m of PVDF/LDPE and PVDF/LDPE-*g*-MAH Blends

PVDF/LDPE (v^{PVDF})	β	ε (10^3 Hz)	E_0 (MV/m)	U_m (J/cm^3)	PVDF/LDPE-*g*-MAH (v^{PVDF})	β	ε (10^3 Hz)	E_0 (kV/mm)	U_m (J/cm^3)
0	10.33	2.35	387.53	1.56	0	9.31	3.18	380.73	2.04
10	23.41	2.93	268.53	0.94	10	24.87	3.53	278.08	1.21
30	9.65	3.94	223.53	0.87	30	34.38	4.80	234.18	1.17
50	8.28	5.53	137.12	0.46	50	16.99	6.26	174.68	0.85
70	10.93	7.77	170.43	0.99	70	14.64	8.98	193.29	1.49
90	9.17	8.36	191.94	1.36	90	30.55	9.06	190.02	1.45
100	13.76	9.14	305.79	3.78	100	13.76	9.14	305.79	3.78

is, the larger of β will be. A better compatibility and a better performance of blends will largely lead to β increasing. As revealed in Table I, the β of PVDF/LDPE-*g*-MAH is larger than that of PVDF/LDPE under each detected v^{PVDF}, indicating a much more homogeneous internal structure in PVDF/LDPE-*g*-MAH blends. Compared with the pure components, moreover, the lower E_b of the PVDF/LDPE blends could be also attributed to the internal voids produced during blending because of the poor compatibility. The E_b of modified LDPE is *ca.* 380.73 kV/mm, decreased by *ca.* 2% comparing with that of pure LDPE of *ca.* 387.53 kV/mm, which is also due to the inner voids caused by MAH molecules. The measured E_b of PVDF/LDPE and PVDF/LDPE-*g*-MAH blends both reach a minimum for the $v^{PVDF} = 50$ vol %. As shown in Table I, limited enhancement of E_b of PVDF/LDPE-*g*-MAH was obtained comparing with that of PVDF/LDPE blends. In this case, not only the size and distribution state of voids but also the addition of polar side group of PE-*g*-MAH should be the important factors determining the E_b of the system. The energy storage density U_m can be described by the formula of:

$$Um = \frac{1}{2}\varepsilon_r\varepsilon_0 Eb^2, \quad (5)$$

where ε_0 and ε_r are the vacuum dielectric constant and relative dielectric constant, respectively. As shown in Table I, the measured U_m of PVDF/LDPE and PVDF/LDPE-*g*-MAH blends both reach a minimum for the $v^{PVDF} = 50$ vol % because of worse compatibility and more significant voids. Compared with PVDF/LDPE blends, the U_m of PVDF/LDPE-*g*-MAH blends were improved on different levels. Thus, considering energy storage and effective cost two factors, $v^{PVDF} = 30$ vol % is the optimal choice.

The Wei bull distribution of E_b of the monolayered and the trilayered films of PVDF/LDPE is also studied, as shown in Figure 10 and Table II. It is revealed that the β of trilayered films are larger than that of monolayered films at all the detected component contents. Similarly, the E_b of the sandwich structure films increases with the content of LDPE, especially for the films with 50 wt % LDPE. These trilayered films were constructed by pure single layer and all the samples for the E_b measurements were molded with equal thickness. Compared with the monolayered films, an enhancement of the E_b is obviously obtained from the trilayered structure films. The less interface defects within trilayered structure films are contributed to improve the E_b owing to the even morphology in each layer, as previously shown in Figure 7. The effective enhancement of the E_b will definitely give to apparent increase of the U_m, especially for the samples with 30, 50, and 70 wt % PVDF. Obviously, both the introduction of MAH and the trilayered structure are beneficial to improve the compatibility and enhance the performance of energy storage.

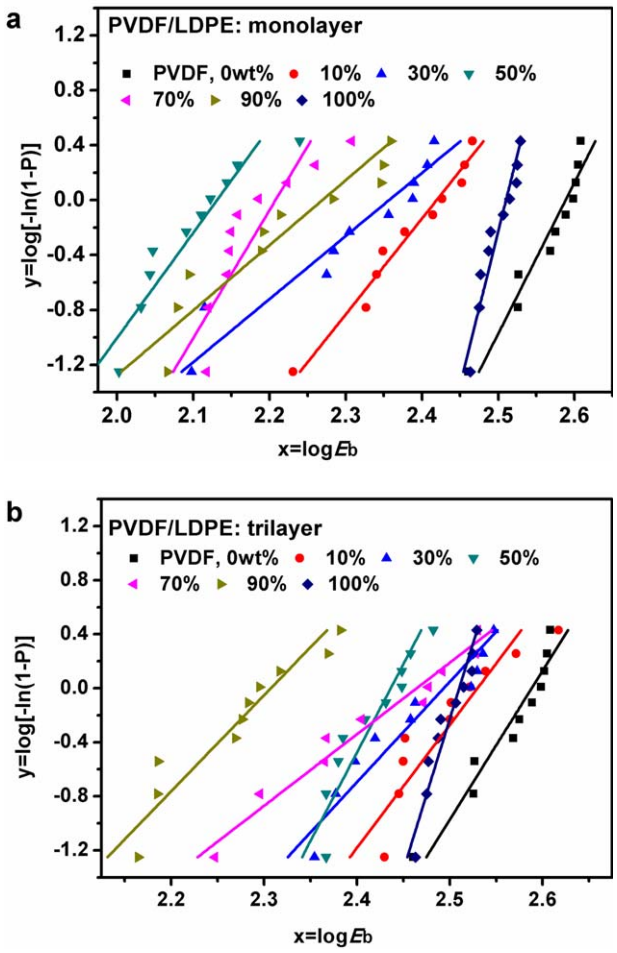

Figure 10. Weibull distribution for E_b of mono-layer and tri-layer films of PVDF/LDPE. [Color figure can be viewed in the online issue, which is available at wileyonlinelibrary.com.]

Table II. The ε, E_0, and U_m of PVDF/LDPE Monolayer and Tri-layer Films

Mono-layer (wt % PVDF)	B	ε (10^3 Hz)	E_0 (kV/mm)	U_m (J/cm^3)	Tri-layer (wt % PVDF)	β	ε (10^3 Hz)	E_0 (kV/mm)	U_m (J/cm^3)
0	10.33	2.35	387.53	1.56	0	10.33	2.35	387.53	1.56
10	6.78	2.53	262.53	0.77	10	7.65	3.02	338.7	1.53
30	4.24	4.46	227.42	1.02	30	6.86	4.95	311.6	2.13
50	9.78	6.06	126.49	0.43	50	13.8	6.13	261.81	1.86
70	6.98	7.22	161.35	0.83	70	6.46	7.78	291.31	2.92
90	4.21	9.07	185.89	1.39	90	6.46	9.41	202.96	1.72
100	20.7	10.1	323.77	4.69	100	20.7	10.1	323.77	4.69

CONCLUSIONS

For improving the dielectric performance, PVDF/LDPE blends were prepared and analyzed in this work. Effects of the compatibility and layered structure on the dielectric properties and breakdown strength were systematically studied. The DSC measurements indicated no chemical reaction or crystal transformation in PVDF/LDPE-*g*-MAH blends, but the MAH could break the crystalline perfection. Morphology of the PVDF/LDPE blends with various volume fractions was similar as insular structure with low PVDF content addition. A narrow co-continuous window of *ca.* 30–50 vol % was observed in terms of the v^{PVDF} and the co-continuous structure became emphasized after grafting with MAH. The increase style of ε of the PVDF/LDPE blends is close to the parallel alignment line and loss tanδ increased correspondingly, which was mainly determined by the content of PVDF and the compatibility between PVDF and LDPE phases. Compared with the pure components, the lower E_b of the blends could be attributed to the voids produced in the system because of the poor compatibility. After introducing LDPE-*g*-MAH into the blends, enhanced ε, E_b and decreased tanδ were observed and the U_m of PVDF/LDPE-*g*-MAH blends were simultaneously improved, in which the $v^{PVDF} = 30$ vol % is the optimal choice for increasing energy storage density with an effective cost. Finally, layered structure of immiscible blends was prepared successfully and found to be helpful to increase ε and E_b, especially for the tri-layered films with $v^{PVDF} = 50$ wt %. This consequence was also attributed to the strong interfacial interaction and the decrease of the internal defects. These PVDF/LDPE-*g*-MAH films with layered structure could be used as a good candidate of dielectric materials with ultrahigh electric-energy-density and low tanδ at high electric fields.

ACKNOWLEDGMENTS

This work was financially supported by Beijing Natural Science Foundation (Grant No. 2142023), National Basic Research Program of China (973 Program, 2014CB239503), National Natural Science Foundation of China (Grant No. 51473018 and 51425201), Ministry of Education of China through Doctor Project (Grant No. 20130006130002), State Key Laboratory of Electrical Insulation and Power Equipments (No. EIPE14204), and the Fundamental Research Funds for the Central Universities (FRF-TP-14-013A1).

REFERENCES

1. Kim, P.; Doss, N. M.; Tillotson, J. P.; Hotchkiss, P. J.; Pan, M. J.; Marder, S. R.; Li, J.; Calame, J. P.; Perry, J. W. *Nano* **2009**, *3*, 2581.
2. Han, R. X.; Jin, J. Z.; Khanchaitit, P.; Wang, J. K.; Wang, Q. *Polymer* **2012**, *53*, 1277.
3. Dang, Z. M.; Yuan, J. K.; Zha, J. W.; Zhou, T.; Li, S. T.; Hu, G. H. *Prog. Mater. Sci.* **2012**, *57*, 660.
4. Barber, P.; Balasubramanian, S.; Anguchamy, Y.; Gong, S.; Wibowo, A.; Gao, H.; Ploehn, H. J.; Zur Loye, H. C. *Material* **2009**, *2*, 1697.
5. Arvidson, S. A.; Roskov, K. E.; Patel, J. J.; Spontak, R. J.; Khan, S. A.; Gorga, R. E. *Macromolecules* **2012**, *45*, 913.
6. Urbaniak-Domagala, W. *J. Appl. Polym. Sci.* **2011**, *122*, 2071.
7. Yang, L. B.; Liu, F. H.; Xia, H. S.; Qian, X. Y.; Shen, K. Z.; Zhang, J. *Carbon* **2011**, *49*, 3274.
8. Liu, Y.; Du, B. X.; Du, D. M. *Int. Trans. Electron. Energ. Syst.* **2013**, *23*, 72.
9. Lau, K.; Vaughan, A.; Chen, G.; Hosier, I.; Holt, A. *J. Phys. D: Appl. Phys.* **2013**, *46*, 303.
10. Crippa, M.; Bianchi, A.; Cristofori, D.; D'Arienzo, M.; Merletti, F.; Morazzoni, F.; Scotti, R.; Simonutti, R. *J. Mater. Chem. C* **2013**, *1*, 484.
11. Xie, L.; Huang, X.; Wu, C.; Jiang, P. *J. Mater. Chem.* **2011**, *21*, 5897.
12. Kobayashi, Y.; Kurosawa, A.; Nagao, D.; Konno, M. *Polym. Eng. Sci.* **2009**, *49*, 1069.
13. He, X.; Yao, K. *Appl. Phys. Lett.* **2006**, *89*, 1.
14. Fan, P.; Wang, L.; Yang, J. T.; Chen, F.; Zhong, M. Q. *Nanotechnol.* **2012**, *23*, 365702.
15. Chen, F.; Bera, D.; Banerjee, S.; Agarwal, S. *Adv. Tech.* **2012**, *23*, 951.
16. Luong, N. D.; Hippi, U.; Korhonen, J. T.; Soininen, A. J.; Ruokolainen, J.; Johansson, L. S.; Nam, J. D.; Sinh, L. H.; Seppala, J. *Polymer* **2011**, *52*, 5237.
17. Wang, S.; Wang, Y. R.; Cheng, K. C.; Hsaio, Y. P. *Ceram. Int.* **2009**, *35*, 265.
18. Brennecka, G. L.; Ihlefeld, J. F.; Maria, J. P.; Tuttle, B. A.; Clem, P. G. *J. Am. Ceram. Soc.* **2010**, *93*, 3935.

19. Martins, P.; Caparros, C.; Goncalves, R.; Martins, P. M.; Benelmkki, M.; Botelho, G.; Lanceros, M. S. *J. Phys. Chem.* **2012**, *116*, 15790.
20. Dang, Z. M.; Lin, Y. Q.; Xu, H. P.; Shi, C. Y.; Li, S. T.; Bai, J. B. *Adv. Funct. Mater.* **2008**, *18*, 1509.
21. Dang, Z. M.; Zheng, Y. *J. Appl. Polym. Sci.* **2008**, *110*, 3473.
22. Mao, Y. P.; Mao, S. Y.; Ye, Z. G.; Xie, Z. X.; Zheng, L. S. *J. Appl. Phys.* **2010**, *108*, 14.
23. Deng, Y.; Zhang, Y.; Wang, Y.; Li, M.; Yuan, J. K.; Bai, J. B. *Compos. Part A* **2012**, *43*, 842.
24. Zhou, W. Y.; Zuo, J.; Ren, W. N. *Compos. Part A* **2012**, *43*, 658.
25. Bao, S. P.; Liang, G. D.; Tong, S. C. *Carbon* **2011**, *49*, 1758.
26. Zhang, Q.; Adebisi, R.; Gladden, J. *Polym. Compos.* **2012**, *33*, 509.
27. He, F.; Lau, S.; Chan, H. L.; Fan, J. *Adv. Mater.* **2009**, *21*, 710.
28. Tang, C. W.; Li, B.; Sun, L. L.; Lively, B.; Zhong, W. H. *J. Eur. Polym.* **2012**, *48*, 1062.
29. Kuang, D. L.; Li, R.; Pei, J. Z. *Polymer* **2014**, *6*, 2146.
30. Yuan, J. K.; Dang, Z. M.; Yao, S. H.; Zha, J. W.; Zhou, T.; Li, S. T.; Bai, J. B. *J. Mater. Chem.* **2010**, *20*, 2441.
31. Dang, Z. M.; Yan, W. T.; Xu, H. P. *J. Appl. Polym. Sci.* **2007**, *105*, 3649.
32. Dang, Z. M.; Zhao, J.; Yin, X. Q.; Shi, J. D.; Zhao, X. D.; Wang, X. Y.; Chen, M.; Hu, G. H. *Sci. Adv. Mater.* **2013**, *5*, 1.
33. Brennecka, G. L.; Ihlefeld, J. F.; Maria, J. P.; Tuttle, B. A.; Clem, P. M. *J. Am. Ceram. Soc.* **2010**, *93*, 3935.
34. Elashmawi, I. S.; Hakeem, N. A. *Polym. Eng. Sci.* **2008**, *1002*, 895.